Article

Synthesis of a Bistable Recuperative Pump Powered by Shape Memory Alloys and a Two-Section Involute Cam

Mihail Kostov [1], Todor Todorov [1] , Rosen Mitrev [2,*] , Georgi Todorov [3] and Konstantin Kamberov [3]

[1] Department of Theory of Mechanisms and Machines, Faculty of Industrial Technology, Technical University of Sofia, 1797 Sofia, Bulgaria; kostovmike@tu-sofia.bg (M.K.); tst@tu-sofia.bg (T.T.)
[2] Department of Logistics Engineering, Material Handling and Construction Machines, Mechanical Engineering Faculty, Technical University of Sofia, 1797 Sofia, Bulgaria
[3] Department of Technology of Machine Tools and Manufacturing, Technical University of Sofia, 1797 Sofia, Bulgaria; gdt@tu-sofia.bg (G.T.); kkamberov@tu-sofia.bg (K.K.)
* Correspondence: rosenm@tu-sofia.bg

Abstract: The paper discusses the synthesis problem of a bistable piston pump, employing a driving mechanism that comprises shape memory alloy wires, a two-section involute cam, and an energy-recuperating spring. The transition from one stable end position to another in the pump is achieved by heating and subsequently shortening one of the shape memory alloy wires, initiating the motion of the mechanism. This is then followed by the engagement of the recuperative spring to traverse the intermediate unstable equilibrium position and complete the entire stroke. The reversal of motion follows a similar approach, where the second SMA wire shortens while the first wire remains in a cold state. Importantly, the mechanism necessitates a low force within the shape memory alloy wire to initiate motion towards the opposite stable position. This research encompasses the examination of type, geometric, and force synthesis considerations for the pump, leading to the development of fundamental kinematic and force relationships. Moreover, a novel mechanism is proposed and synthesized, incorporating a two-section involute cam with a cusp point, to generate the desired discontinuous moment function produced by the recuperative spring. Further analysis reveals that the thermal time constant, which regulates the dynamic response of the mechanism, is directly proportional to the diameter of the driving SMA and inversely proportional to the square root of the number of SMA branches.

Keywords: synthesis; bistable mechanism; shape memory alloys; reciprocating pump; energy recuperation; two-section involute cam

1. Introduction

The application of smart materials in advanced actuators and sensor systems has exhibited a steady increase over the past two to three decades. This is primarily due to the ability of smart materials to provide unique solutions to engineering challenges while optimizing material consumption [1]. Moreover, the incorporation of smart materials has resulted in improved dynamics and energy efficiency in the newly developed products.

Shape memory alloys (SMAs) are a typical representative of smart materials that provide opportunities to create actuators with substantial force generation and displacement capabilities, spanning from microns to several millimeters. Despite the persistent research efforts in SMA [2–4], the most widely adopted alloys in commercial applications are currently NiTi alloys, characterized by a nickel and titanium composition of approximately 50% [5,6].

Within modern engineering, SMAs find extensive application through their three distinct effects: the Super Elastic Effect, the Two-Way Shape Memory Effect, and the One-Way Shape Memory Effect [7,8]. The Super Elastic Effect pertains to the restoration of the material's shape at a constant temperature and is not commonly employed in

actuators. The Two-Way Shape Memory Effect enables changes in the material's form in response to temperature stimuli and is predominantly utilized in microelectromechanical systems, while its implementation in macroelectromechanical systems is relatively less frequent [9–11].

The One-Way Shape Memory Effect requires pre-deformation of the SMA driving element through the application of a biasing force, which can be achieved by employing a constant force (such as weight), a linear force (such as elasticity), or by utilizing an opposing SMA element with temperature control [12–16]. The pre-deformation corresponds to the displacement of the actuator's executive unit in a specific direction. Upon heating, the driving SMA element re-establishes its original shape, resulting in the movement of the executive unit in the opposite direction. After heating, SMA drive elements can successfully recover their initial shape despite undergoing substantial deformations, encompassing tensile, compressive, bending, torsional, or mixed deformations [17,18].

The actuators that deflect SMA wires using a spring mechanism represent the widely adopted and uncomplicated design approach. Typically, the heating of SMA wires is achieved by means of an electric current, harnessing the Joule's Effect [19]. These actuators are the most compact, as SMA wires provide the highest energy density. Their movement is smoothly controlled and noiseless. In many instances, these actuators can provide engineering solutions superior to conventional ones, such as motor-driven spur gears, lever mechanisms, or pneumatic or hydraulic cylinders [20]. Despite the well-established advantages associated with the SMA drive, particularly in the context of microactuators, it is imperative to acknowledge the presence of certain inherent limitations. It is undeniable that SMA devices exhibit low energy efficiency, with reported efficiencies of 2–3% for the SMA heat engine [21] and up to 4.5% for the clamp-free actuator [22]. This calls for further investigation and improvement in order to optimize their performance.

Bistable mechanisms exhibit two distinct stable equilibrium positions, between which they transition through an intermediate unstable equilibrium position, driven by changes in elastic forces [23–25]. These mechanisms are suitable for application in electrical circuit contacts and the creation of nonlinear oscillation systems due to their rapid switching after passing the unstable equilibrium position [26,27]. The operation of elastic forces can generate restoring (recuperating) forces [28]. Bistable mechanisms are appropriate for driving through SMAs because only half of the stroke can be overcome to the unstable position. This is achieved by deviating the bistable mechanism from one of its stable positions to the unstable one with SMAs and then releasing it to move by the action of the elastic forces [29].

The team of authors behind this paper has developed and patented a valve featuring bistable action, whereby half of the work required for valve closure or opening is effectively supported by an energy-recuperating spring [30,31]. Electric heating of the SMA wires is employed to initiate the partial displacement of the executive element in this valve. A design for a piston pump that uses the bistable valve principle has been developed in [32]. This pump achieves bistability and energy recuperation by utilizing a three-arm rocker and a recuperative spring. A patent application [33] has been filed to protect the structure and principle of operation. Based on energy and force calculations, it has been determined that the design of the bistable SMA-driven pump proposed in reference [32] can be further improved. One possibility is the introduction of an additional cam mechanism for converting the recuperative force by a suitable non-linear function.

This paper aims to explore various possibilities regarding the type, force, and geometric synthesis of a bistable piston pump, employing a driving mechanism that comprises SMA wires, a two-section involute cam, and an energy-recuperating spring to achieve optimal performance. This design should eliminate the shortcomings of the mentioned bistable pump with a three-arm rocker and a recuperative spring, developed in [32]. Additionally, the electrothermal drive system of the piston pump will be investigated, with the ultimate goal of achieving a fast dynamic response. By delving into these aspects, this research contributes to advancing the field and enhancing the efficiency of SMA-driven bistable

piston pumps, with potential applications in different areas, including fluid power systems and actuation mechanisms.

2. Motivation for Creating a Bistable Pump with Coinciding Unstable Equilibrium Positions

Figure 1 depicts a simplified kinematic sketch of the bistable reciprocating piston pump, as proposed in references [32,33], incorporating a three-arm rocker, a recuperative spring, and a drive mechanism that employs SMA.
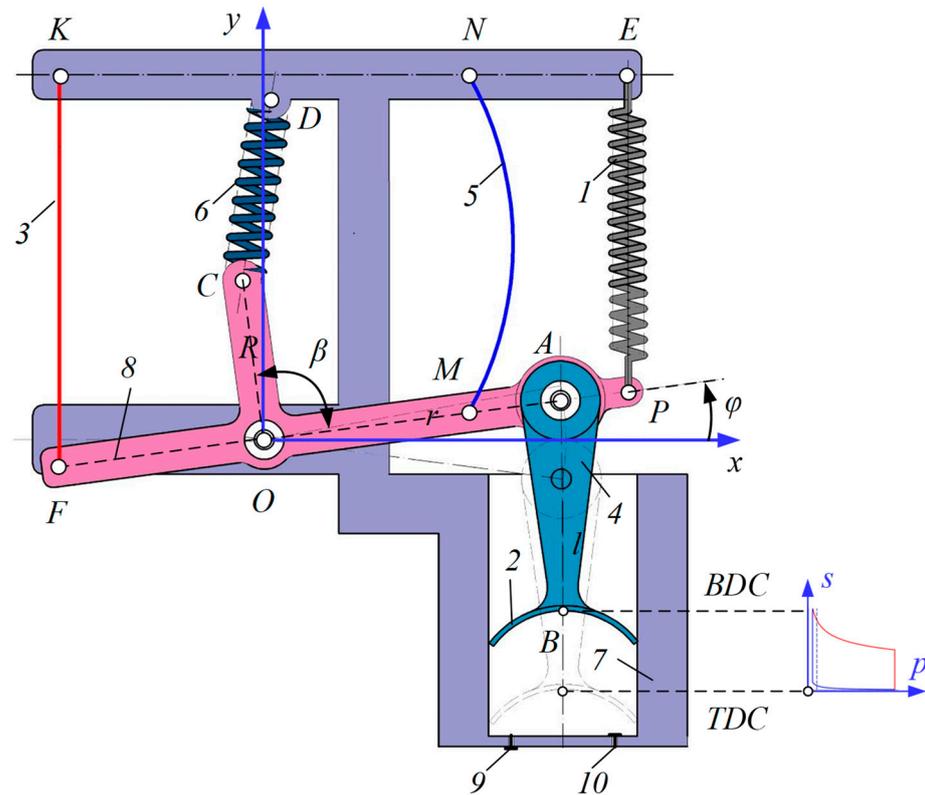
Figure 1. Kinematic scheme of the bistable pump with recuperative springs [32,33]: 1. Piston spring; 2. Piston; 3. Discharge SMA wire; 4. Coupler; 5. Suction SMA wire; 6. Recuperative spring; 7. Piston cylinder; 8. Three-arm rocker; 9. Discharge valve; 10. Suction valve.

The geometric and force parameters of the pump are precisely determined to ensure stable equilibrium at two specific positions, presented in Figure 1: the bottom dead center (BDC) and the top dead center (TDC) of piston 2. The same figure illustrates the alignment between BDC and TDC and the corresponding positions on the indicator diagram, presented in pressure-displacement coordinates *p-s*.

The bistability originates from the alteration in sign of the resultant moments about the revolute joint at point *O*, resulting from the active forces exerted by the piston and the springs on the three-arm rocker 8. This ensures that an unstable equilibrium position is present during both the discharge and suction periods. Fine-tuned adjustments to this unstable equilibrium position can be accomplished by manipulating the characteristics of the piston spring 1.

The ideal operation of the bistable pump is based on the principle that the two SMA wires, 3 and 5, displace the rocker to an unstable equilibrium position, from which the recuperative spring 6 aids further movement. It is crucial to highlight that the extension of the SMA wires should be limited to the point of instability, rather than spanning the entire piston stroke. Beyond this point, the active wire relaxes, and the tension is transferred to the opposing SMA wire through the recuperative spring.

It is noteworthy that the unstable equilibrium positions for the suction and discharge phases in general may differ. However, in certain conditions, such as those found in the bistable valve [30,31], these positions can coincide. In order to determine the unstable equilibrium positions, it is imperative to conduct a thorough force analysis of the mechanism.

Given that the origin of the global coordinate system {xy} is located at point O (see Figure 1), the conversion from piston displacement s to position angle φ of the three-arm rocker is achieved through the utilization of the following equation, which represents the position function of the slider-crank mechanism:

$$s = h_p + c_l + r \sin \varphi - r\sqrt{l^2 - (r \cos \varphi - x_B)^2} - y_{BDC} \tag{1}$$

where h_p is the piston stroke, c_l is the pump clearance, $r = OA$ is the length of the first arm of the three-arm rocker, $l = AB$ is the length of the coupler, and y_{BDC} is the BDC coordinate of the piston.

Equations (2)–(14), derived in [32], can be utilized to obtain the force characteristics of the system.

The position of point C is determined by its coordinates

$$x_C = R\cos(\varphi + \beta) \tag{2}$$

$$y_C = R\sin(\varphi + \beta) \tag{3}$$

where $R = OC$ and $\beta = \sphericalangle AOC$.

The recuperative spring length CD is denoted by ρ expressed as

$$\rho = CD = \sqrt{(x_C - x_D)^2 + (y_C - y_D)^2} \tag{4}$$

The axial force F_r in the recuperative spring is found from the expression

$$F_r = (l_{R0} - \rho)k_r \tag{5}$$

where l_{R0} and k_r are the initial nondeformed length of the recuperative spring, and its stiffness, correspondingly.

The moment M_r of the force F_r with respect to the joint O is

$$M_r = -F_r h_r \tag{6}$$

where $h_r = OC_1$ is the distance between the line of action of the recuperative force and point and $OC_1 \perp DC_2$.

From the triangle ΔOC_1C_2, after denoting $x_r = OC_2$ and $\psi_r = \sphericalangle C_1OC_2$ the distance h_r is expressed as:

$$h_r = x_r \cos \psi_R \tag{7}$$

where the cosine of the angle between the ordinate and the direction of the recuperative force can be found from

$$\cos \psi_r = \frac{y_D - y_C}{\rho} \tag{8}$$

and for x_r is valid the formula:

$$x_r = x_D + y_D \tan \psi_r = x_D + y_D \frac{x_C - x_D}{y_D - x_C} \tag{9}$$

The piston spring force F_s is expressed by the following equation:

$$F_s = \left[(y_E - r_p \sin \varphi) - l_{s0}\right]k_s \tag{10}$$

which expresses that the piston spring force pulls the piston during the suction stroke, according to the presented schematic diagram and assuming $x_E = r_p \cos \varphi_{in}$. In Equation (10) l_{s0} is the initial length of the piston spring, y_E is the vertical coordinate of point E, k_s is the stiffness of the piston spring, and $r_p = OP$.

The moment of the piston spring force with respect to point O is:

$$M_s = F_s r_p \cos \varphi \tag{11}$$

The pressure p of the gas during the suction stroke creates a piston gas force F_p which depends on the indicator diagram and is presented by the formula

$$F_p = \frac{\pi D^2}{4} (p - p_{atm}) \tag{12}$$

where D is the diameter of the piston, and p_{atm} is the atmospheric pressure.

The angle γ between the vertical axis and the direction of the coupler is:

$$\gamma = \arcsin \frac{r \cos \varphi - x_{B2}}{l} \tag{13}$$

where $x_{B2} = r \sin \varphi_0$ and $l = BD$.

The moment M_p of the piston force F_p with respect to point O is calculated using the angle γ as follows:

$$M_P = -F_p r \cos \gamma \tag{14}$$

The pressure acting on the piston is assumed to be pre-set and is represented by the pressure-displacement indicator diagram shown in Figure 2a [32], where the following positions are used to denote the parts of the diagram: 1—compression, 2—discharge, 3—expansion, and 4—suction. The red line represents the motion of the piston from TDC to BDC, whereas the blue line represents the motion from BDC to TDC. The moment M_p generated by the indicating pressure force at the revolute joint O of the three-arm rocker is computed using Equation (14) and is depicted in Figure 2b.
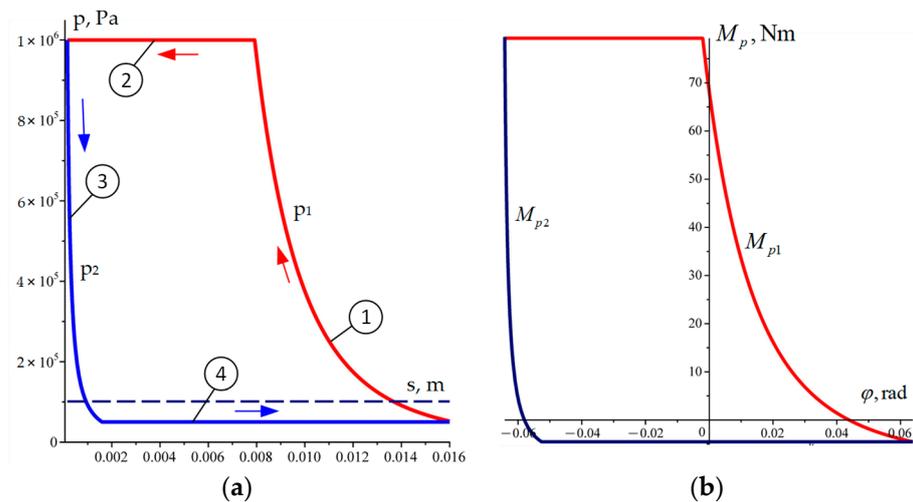
Figure 2. Indicator diagram: (**a**) In pressure-displacement coordinates p-s [32]; (**b**) In coordinates moment-angle of rocker arm M_p-φ.

Figure 3a depicts the graph of a linear recuperating spring moment M_r (plotted with the opposite sign) and the pressure moments M_{p1} and M_{p2} represented by the indicator diagram. The two instability points, labeled as φ_{ui} for the discharge period and φ_{us} for the suction period, are determined by the intersection of the line representing the recuperative force moment M_r and the indicator diagram.
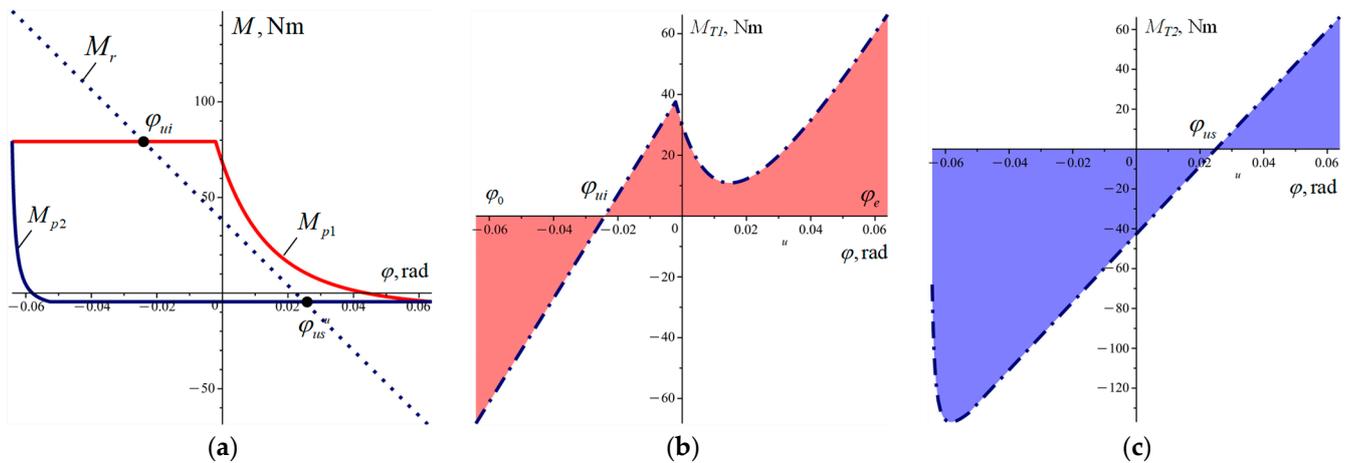
Figure 3. Recuperation by a spring with a linear characteristic: (**a**) View of the linear characteristic and indicator diagram; (**b**) Resultant moment for the discharge period after the recuperation; (**c**) Resulting moment for the suction period after the recuperation.

The graph demonstrates that for the two instability angular positions to coincide, the characteristic of the recuperative moment must be a vertical line. However, attaining bistability in such a scenario would necessitate a recuperative spring with an infinitely large stiffness, which is not practically achievable. The practical solution reached in [32] employs a spring with exceptionally high stiffness, resulting in excessively large reaction forces among the pump components. Furthermore, the extensions of the hot and cold SMA wires would overlap during the interval from φ_{ui} to φ_{us}, leading to increased energy consumption.

The graphs of the total moments $M_{T1} = M_{p1} - M_r$ and $M_{T2} = M_{p2} - M_r$ for the discharge and suction periods, respectively, are shown in Figure 3b,c. From both graphs, it can be seen that maximum absolute values of the total moments were obtained at the initial point φ_0 and the end point φ_e. At these two points, the extreme total moments are balanced by the forces of the SMA wires, thus achieving two stable pump equilibria for the suction and the discharge. In both graphs of Figure 3b,c there is one zero value of the total moment φ_{ui}, and φ_{us}, which means that there is an unstable equilibrium at this position. When the two unstable equilibrium positions are located in the middle of the rotation angle interval, the two SMA wires will only deform to half of the piston stroke, which turns out to be optimal for energy consumption. However, this condition requires that the intersections φ_{ui}, and φ_{us} in Figure 3a are above each other, which is equivalent to a vertical characteristic of the recuperating moment.

3. Formulation of the Task for the Synthesizing of a Driving Mechanism

In order to avoid the drawback of the three-arm rocker pump scheme analyzed in Section 2, a mechanism should be synthesized that reduces the difference in the two unstable equilibrium positions (see Figure 3a). It is suggested that this be achieved by assuming that the moment of the recuperative force should change according to the following reference piecewise function

$$M_r^* = \begin{cases} M_{p1m} + (\varphi - \varphi_0)k_1 & if \quad \varphi_0 \le \varphi \le \varphi_{ci} \\ \frac{M_{p1m} - M_{p2m}}{\varphi_{ui} - \varphi_{us}}\varphi & if \quad \varphi_{ci} \le \varphi \le \varphi_{cs} \\ M_{p2m} + (\varphi - \varphi_0)k_2 & if \quad \varphi_{cs} \le \varphi \le \varphi_e \end{cases} \tag{15}$$

where M_{p1m} and M_{p2m} are the values of the discharge and suction sectors of the reference function at $\varphi = \varphi_0$, k_1 and k_2 are the stiffnesses of the first and third part of M_R^*, and φ_{ci} and φ_{cs} are the intersection points. If a mechanism is synthesized to generate a recuper-

ative function close to the relationship (15), much of the listed drawbacks of the linear recuperative force will be avoided.

In Figure 4a, the negative recuperative moment M_r^* is depicted using a dashed line, while the indicator diagram is represented by a solid line. In Figure 4b,c, the changes of the piston moments M_{p1}, M_{p2} and total moments $M_{T1} = M_{p1} - M_r^*, M_{T2} = M_{p2} - M_r^*$ are shown. The presence of a jump discontinuity in the middle of the two strokes facilitates the alignment of the two instability positions φ_{ui} and φ_{us}. This approach successfully addresses the challenges mentioned earlier by minimizing the stretching of the SMA wires and utilizing springs with low stiffness and low loading forces.
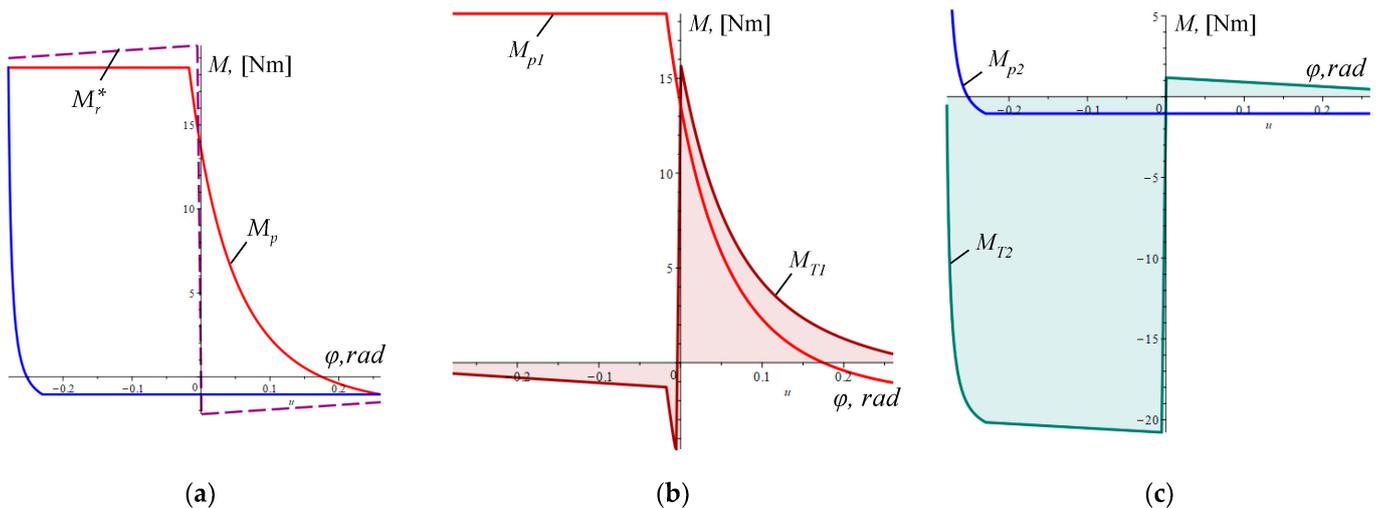
Figure 4. Influence of the recuperative moment on work distribution (shaded areas): (**a**) Indicator diagram and the reference recuperative moment; (**b**) Work of the reference recuperative moment and piston moment at discharge period; (**c**) Work of the reference recuperative moment and piston moment at suction period.

The implementation of the proposed discontinuous reference function requires a different mechanism than the one that incorporates a three-arm rocker (refer to Figure 1). Various mechanical structures are possible, and the determination of the suitable number of links and their types falls within the subject of the "Theory of Mechanisms and Machines" [34]. Among all possible solutions, the cam mechanism in Figure 5 was chosen due to its relatively simple structure. A similar idea is suggested in [33]. The design of such a mechanism is as follows (see Figure 5). The cam 1 is produced on the three-arm rocker 8, and it comes into contact with a roller 9 that is mounted on the rotating follower 7 through a revolute joint. The follower and pump body are connected by a recuperative spring 6.

The spring 6 applies a non-linear force that results in a transmission of a non-linear moment to the three-arm rocker through the cam profile. This cam mechanism differs from the conventional cam mechanisms because the cam and the follower interchange function as actuator and actuated link. Initially, the three-arm rocker and cam are rotated by the SMA wires until the mechanism reaches the unstable position. Subsequently, the movement is sustained by the recuperative spring to complete the stroke.

The synthesis of the cam mechanism that will realize the proposed discontinuous reference function will be performed under previously assumed constant numerical values of the parameters of the indicator diagram (see Figure 2), the dimensions of the slider—crank mechanism, and the piston stroke and diameter. The numerical values of these parameters are shown in Table 1.
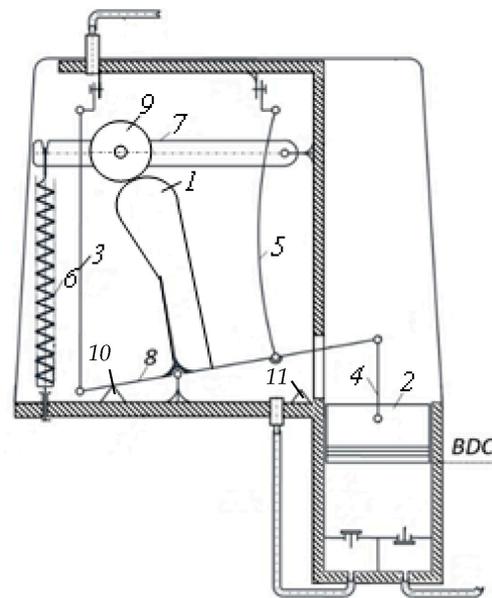
Figure 5. Scheme of a pump with a recuperative cam mechanism: 1. Cam; 2. Piston; 3. Discharge SMA wire; 4. Coupler; 5. Suction SMA wire; 6. Recuperative spring; 7. Oscillating follower; 8. Three-arm rocker; 9. Roller; 10. Left end stop; 11. Right end stop.

Table 1. Constant numerical values of the pump parameters.

Parameter	Symbol	Unit	Value
First arm of the three-arm rocker	OA, r	m	0.125
Coupler	AB, l	m	0.0415
Starting rocker angle	φ_0	rad	−0.0639
Starting rocker angle in degrees	φ_{0d}	deg	−3.66
Piston diameter	D_p	m	0.03
Distance from point O to sliding line of center of the piston	x_B	m	0.0290
Piston stroke	h_p	m	0.016
Vertical piston position at BDC	y_{BDC}	m	−0.034
Maximum discharge pressure	$p_{H\_}$	Pa	1,000,000
Maximum suction pressure	$p_{l\_}$	Pa	50,000
Maximum discharge moment	M_{p1max}	Nm	79.24
Minimum suction moment	M_{p2max}	Nm	4.53

4. Synthesis of a Two-Section Involute Cam Profile

Figure 6 presents the cam profile necessary to generate the required reference piecewise characteristic for the recuperating moment. The cam profile consists of two involutes, denoted as left involute (E_l) and right involute (E_r), with concentric base circles k_l and k_r, respectively. The involute cam was originally introduced by Shaw [35,36]. The three-arm rocker rotates around the center of the revolute joint O, which coincides with the centers of the two base circles. The involute's property, where its normal is tangential to the base circle, is utilized to ensure a constant force arm between the roller and the cam. The transition between the two sections of the involute is accomplished by a cusp point P_m.
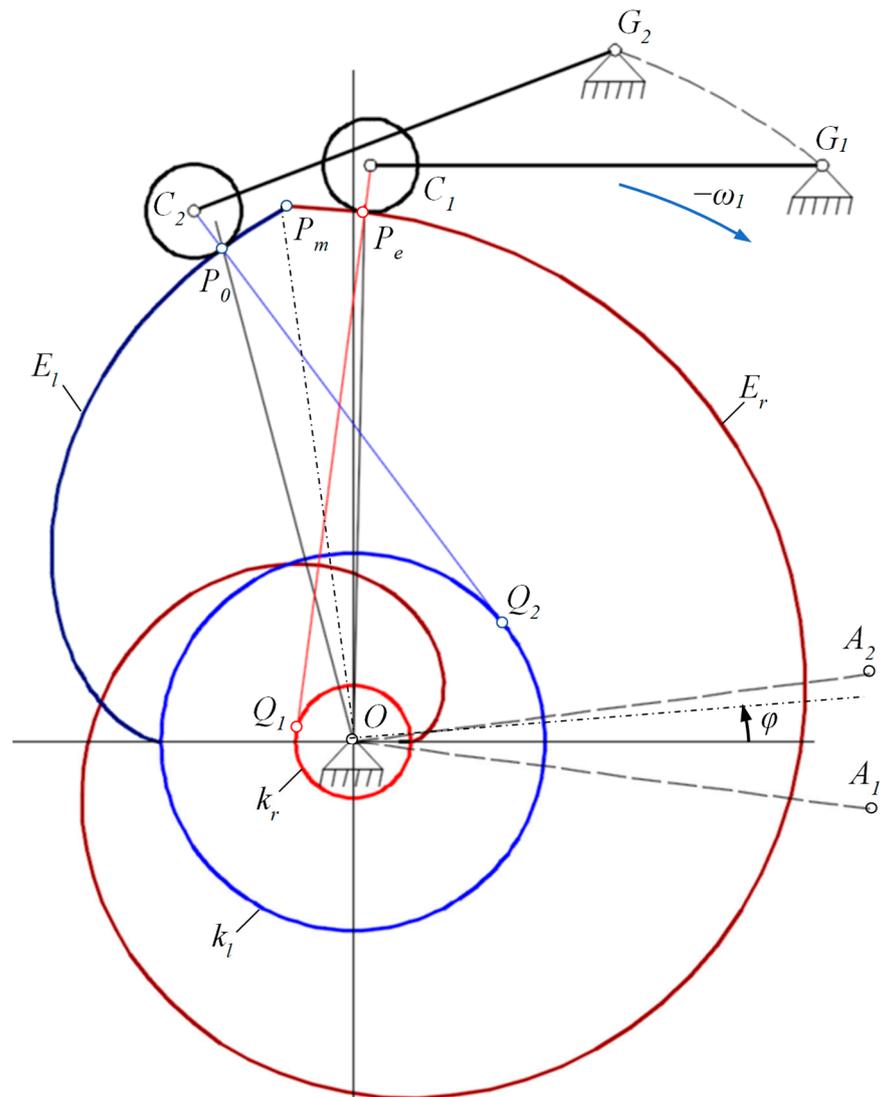
Figure 6. Profile of the two-section involute cam.

The two rocker positions $G_1 C_1$ and $G_2 C_2$ are obtained by the method of the inversion of the frame with the rocker rotated opposite to the direction of the angular velocity ω_1 of the three-arm rocker.

The cam profile comprises two sections: $P_0 P_m$, which is a part of the left involute, and $P_m P_e$, which is a part of the right involute. The cusp point P_m is formed by the intersection of these two involutes, and it is advisable to align this position of the cam when $\varphi = 0$, based on the assumed reference moment conventions. The ratio of the radii of the base circles is chosen to be equivalent to the ratio of the extreme values of the reference recuperative moment. Since the common normals at the contact points between the roller and cam are always tangential to the base circles, the transformed force arm of the recuperating spring will be equal to one of these radii.

Examining Figure 6, it can be observed that when φ varies from φ_0 to 0, representing the contact at the left involute in the $P_0 P_m$ section, the force is transmitted along the normal $C_2 Q_2$. In this case, the force arm corresponds to the radius of the larger base circle of the left involute, resulting in a positive moment. As the contact is at the $P_m P_e$ section, the force is transmitted along the normal $C_1 Q_1$, leading to a negative moment, while the force arm changes to the smaller radius of the right involute.

By incorporating the two involutes in the cam profile, the issue of discontinuity in the recuperating moment function is resolved. Moreover, a change in the sign and magnitude of the moments for the two sections is achieved.

5. Synthesis of a Bistable Pump Containing a Two-Section Cam

The synthesis of the pump mechanism must meet three fundamental requirements. Firstly, it should achieve bistability, allowing for two stable end positions. Secondly, it should amplify the force exerted by the recuperative spring. Lastly, it should convert the spring force in accordance with the pre-set reference non-linear function.

The schematic diagram in Figure 7 portrays the modified mechanism depicted in Figure 1, which incorporates a two-section involute cam. The essential components of the mechanism remain unchanged from those depicted in Figure 1. The recuperative spring is suspended between the body and the oscillating follower *DCG* in points *E* and *D*.
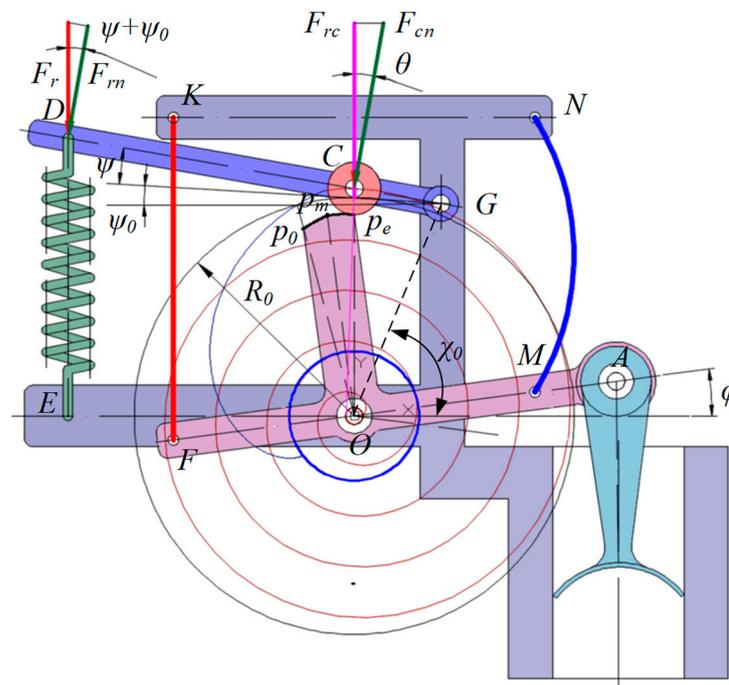
Figure 7. Schematic diagram of the bistable pump with two-section involute cam and oscillating follower.

The force of the spring is transmitted to the cam by a roller which rotates around point *C*. According to Figure 7, the cam is located on the third arm of the three-arm rocker with two involute sections with different base circles. The drawing shows the involutes of the pitch profile which, as known from the properties of the involute, is equidistant from the cam profile. For the discharge phase, the three-arm rocker is first rotated by the wire *KF* from the end position φ_e to the unstable discharge position φ_{ui}. The roller contacts the involute with a small radius of the base circle during this time, resulting in a small moment arm of the forces of the SMA wire. The SMA wire has fully recovered its elongation after the instability point and cannot drive the three-arm rocker anymore. Then, the driving is performed by the spring, since the cam has already changed the involute profile, which changes the sign and the amount of recuperative moment. The SMA wire *NM* is stretched and the SMA wire *FK* is relaxed during this period. After that, a voltage is applied to the ends of wire *NM*, which causes it to heat up and shrink. This signifies the start of the suction period. The SMA wire *NM* rotates the three-arm rocker from angle φ_0 to the suction instability angle φ_{us}. Due to the rotation of the three-arm rocker after the suction instability angle φ_{us}, the SMA wire *NM* relaxes, its voltage is turned off, and it begins to cool. The rotation of the three-arm rocker continues in the same direction under the action of the

recuperating spring, which reverses the direction of its moment due to a change in the involute of the cam. During this rotation, the SMA wire FK is stretched, which sets up the mechanism to repeat the discharge period. The presence of two stable end positions is ensured by the reactions of each SMA wire in a cold tensioned state.

The force F_{rc} with which the roller presses the cam after considering the balance of the moments of the forces acting on the secondary rocker relative to point G is obtained as:

$$F_{rc} = \left(1 + \frac{l_{r1}}{l_{r2}}\right) F_r \cos(\psi + \psi_0) \cos \theta \tag{16}$$

where $l_{r1} = DC$, $l_{r2} = CG$, F_r is the force of the recuperative spring, θ is the pressure angle, ψ is the output cam angle, and ψ_0 is the initial output cam angle (Figure 7).

The moment M_{rs} of the recuperative spring force with respect to point O is

$$M_{rs} = F_{rc}r_b = r_b\left(1 + \frac{l_{r1}}{l_{r2}}\right) F_r \cos(\psi + \psi_0) \cos \theta \tag{17}$$

where $r_b = \begin{cases} -r_l & if \quad \varphi \in [\varphi_0, 0] \\ r_r & if \quad \varphi \in [0, \varphi_e] \end{cases}$ is the radius of the base involute circle.

The spring force F_r is expressed as

$$F_r = F_{r0} + l_r(\tan \psi - \tan \psi_0)k_r \tag{18}$$

where $l_r = l_{r1} + l_{r2} = DG$, F_{r0} is the initial spring force, and k_r is the spring stiffness.

The output angle of the cam mechanism is determined by the relationship.

$$\psi = \pi - \arccos\left(\frac{x^2 + y^2 - d_f^2 - l_{r2}^2}{2d_f l_{r2}}\right) - \chi_0 \tag{19}$$

where $d_f = OG$ and $\chi_0 = \sphericalangle GOx$. The coordinates of the cam profile can be left x_l, y_l or right x_r, y_r oriented, assumed as $x = \begin{cases} x_l & if \; \varphi \in [\varphi_0, 0] \\ x_r & if \; \varphi \in [0, \varphi_e] \end{cases}$, $y = \begin{cases} y_l & if \; \varphi \in [\varphi_0, 0] \\ y_r & if \; \varphi \in [0, \varphi_e] \end{cases}$ and calculated according to the type of profile. For the left involute, they are presented as:

$$\begin{aligned} x_l &= -r_l[\cos(t_l + a_l) + t_l \sin(t_l + a_l)] \\ y_l &= r_l[\sin(t_l + a_l) - t_l \cos(t_l + a_l)] \end{aligned} \tag{20}$$

and for the right involute, the profile coordinates are obtained in the form

$$\begin{aligned} x_r &= r_r[\cos(t_r + a_r) + t_r \sin(t_r + a_r)] \\ y_r &= r_r[\sin(t_r + a_r) - t_r \cos(t_r + a_r)] \end{aligned} \tag{21}$$

where r_l, r_r are the radii of the base left and right involute, t_l and t_r are the parameters for left and right involute, and a_l, a_r are constants for the left and right involute that determine the position of the initial point on the base circle.

After substituting (17) in (18), the recuperative moment is expressed as

$$M_{rs} = r_b\left(1 + \frac{l_{r1}}{l_{r2}}\right)[F_{r0} - l_r(\tan \psi - \tan \psi_0)k_r]\cos(\psi + \psi_0)\cos \theta \tag{22}$$

where $r_b = \begin{cases} -r_l & if \; \varphi \in [0, \varphi_e] \\ r_r & if \; \varphi \in [\varphi_0, 0] \end{cases}$ is the radius of the involute cam base circle.

For the synthesis of the bistable cam mechanism, it is assumed that for the position of the tree-arm rocker $\varphi = 0$ the roller contacts the cam at the middle point p_m. Then, the arms EO and OA are horizontal and the third arm Op_m is vertical (see Figure 8). Here the middle

point p_m of the cam profile lies on the ordinate Oy. Assuming also that in this position the output angle $\psi = 0$, the radius R_0 of the cam pitch circle must be

$$R_0 = y_{p_m} + r, \tag{23}$$

where $y_{p_m} = Op_m$ is the ordinate of the middle point p_m of the cam profile and r is the radius of the roller. For such a configuration of the mechanism (Figure 8), it is evident that when the input angle $\varphi = 0$ then the angles are:

$$\psi = 0, \quad \theta = \theta_0, \quad and \quad \psi_0 = 0. \tag{24}$$
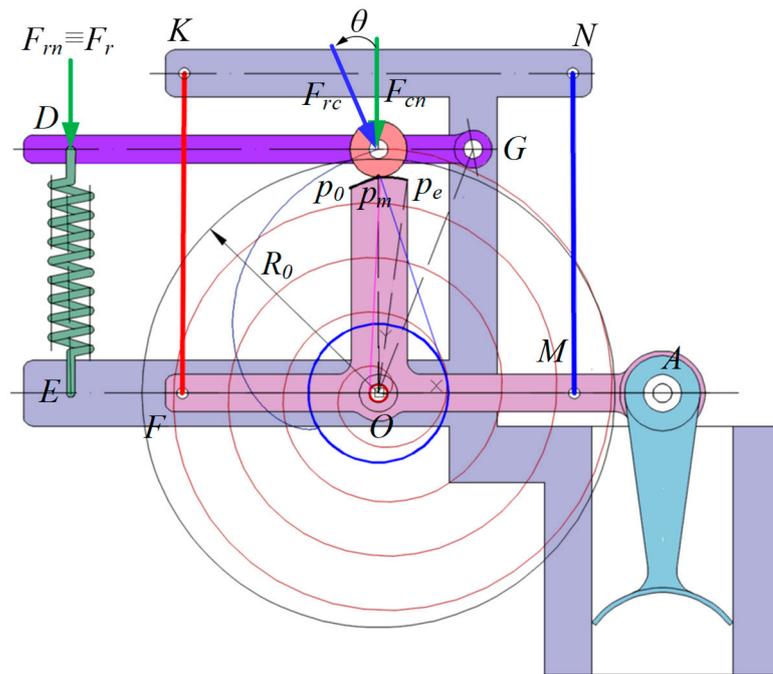
Figure 8. Schematic diagram of the pump bistable mechanism with two-section involute cam and oscillating follower in horizontal position of the rocker's arm *OA*.

The Equation (22) is transformed in the form

$$M_{rs|\varphi=0} = r_b\left(1 + \frac{l_{r1}}{l_{r2}}\right)F_{r0}\cos\theta_0 \tag{25}$$

The Equation (25) is suitable for the force and geometric synthesis of the mechanism. First, the radius r_l of the base circle of the left involute can be selected. Next is the choice of the ordinate y_{p_m} of the middle point $P_m(0, y_{p_m})$ of the cam. The left involute parameters follow from the system.

$$\begin{aligned} r_r[\cos(t_r + a_r) + t_r\sin(t_r + a_r)] &= 0 \\ r_r[\sin(t_r + a_r) - t_r\cos(t_r + a_r)] &= y_{p_m} \end{aligned} \tag{26}$$

which leads to the solution

$$\begin{aligned} a_r &= \arctan_2\left[\frac{r_r}{y_{pm}}, -\sqrt{1 - \left(\frac{r_r}{y_{pm}}\right)^2}\right] \\ t_r &= \sqrt{\left(\frac{y_{pm}}{r_r}\right)^2 - 1} \end{aligned} \tag{27}$$

The radius of the right base circle is determined by the ratio

$$\frac{r_r}{r_l} = \frac{M_{r\min}}{M_{r\max}} \tag{28}$$

The parameters of the left involute circle follow from the system

$$\begin{aligned} -r_l[\cos(t_l + a_l) + t_l \sin(t_l + a_l)] &= 0 \\ r_l[\sin(t_l + a_l) - t_l \cos(t_l + a_l)] &= y_{p_m} \end{aligned} \tag{29}$$

which is solved to

$$\begin{aligned} a_l &= \arctan_2\left[\frac{r_l}{y_{pm}}, \sqrt{1 - \left(\frac{r_l}{y_{pm}}\right)^2}\right] \\ t_l &= \sqrt{\left(\frac{y_{pm}}{r_l}\right)^2 - 1} \end{aligned} . \tag{30}$$

The amplification of the spring recuperative force depends on ratio $m_{12} = \frac{l_{r1}}{l_{r2}}$ which along with the length of the secondary rocker arm l_r is chosen for reasons of appropriate design. The initial force of the recuperative spring can be found from (25) in the form

$$F_{r0} = \frac{M_{r\max}}{r_r(1 + m_{12})\cos\theta_0} \quad or \quad F_{r0} = \frac{|M_{r\min}|}{r_l(1 + m_{12})\cos\theta_0} \tag{31}$$

In the current synthesis, the stiffness of the recuperative spring is found for the angular position $\varphi = \varphi_e = 0.260$ rad. In this position the roller contacts with point p_c of the right involute, which is rotated relative to the zero position of the angle $-\varphi_e$. The parameter t_{rc} of the right involute is found by a numerical solution of the equation

$$\frac{y_{rc}(t_{rc})}{x_{rc}(t_{rc})} = \frac{\sin(t_{rc} + a_r) - t_{rc}\cos(t_{rc} + a_r)}{\cos(t_{rc} + a_r) + t_{rc}\sin(t_{rc} + a_r)} = \tan(-\varphi_e) \tag{32}$$

The next step of synthesis is to find the output angle $\psi_c = \psi(-\varphi_e)$ using (17) where $x = y_{rc}$ and $y = y_{rc}$ are substituted. To avoid the multiple solutions, including those of complex number type, it is recommended to search for the roots of the Equation (30) in an interval close to $\psi_c \in [(1 - \delta)\psi(0), (1 + \delta)\psi(0)]$, where $\delta = 0.01$ and $\delta = 0.1$, respectively, for the right and left evolute. Considering that $\psi_0 = 0$ the stiffness of the spring is expressed from (10) as

$$k_r = \frac{1}{l_r \tan\psi_c}\left[\frac{M_r(\varphi_e)}{r_b(1 + m_{12})\cos\psi_c\cos\theta} - F_{r0}\right], \tag{33}$$

where the pressure angle θ after substituting $\psi = \psi_c$ is calculated from

$$\theta = \beta - \frac{\pi}{2} + \alpha, \tag{34}$$

where

$$\beta = \arcsin\left[\frac{d_f}{R + r}\sin(\psi + \chi_0)\right], \tag{35}$$

and

$$\alpha = \pm\arcsin\frac{r_b}{R}. \tag{36}$$

The angle χ_o determines the position of the fixed revolute joint G, e.g., $\chi_o = \angle GOx$ and the radius of the involute is $R = \sqrt{x^2 + y^2}$, where r is the radius of the roller.

Numerical values of the parameters obtained from the synthesis are shown in Table 2. The sign "+" in α is assumed for the right involute and "-" is for the left involute.

Table 2. Numerical results from the force and geometric synthesis.

Parameter	Symbol	Unit	Value
Small arm of the oscillating follower	GC, l_{r2}	m	0.02
Large arm of the oscillating follower	CD, l_{r1}	m	0.065
Oscillating follower ratio	m_{12}	-	3.25
Length of the oscillating rocker	CG, lr	m	0.085
Radius of the involute at $\varphi = 0$	y_{pm}	m	0.046
Radius of the right base circle	r_r	m	0.00086
Radius of the left base circle	rl	m	0.015
$\angle GOx$	χ_0	rad	1.2019
Initial force of the recuperative spring	F_{r0}	N	403.7
Stiffness of the recuperative spring	k_r	N/m	9947.7
First gradient for aim recuperative moment	k_1	Nm/rad	19.1
Second gradient for aim recuperative moment	k_2	Nm/rad	2.7
Value at $\varphi = 0$ of first aim recuperative moment	M_{p1m}	Nm	19.08
Value at $\varphi = 0$ of second aim recuperative moment	M_{p2m}	Nm	−2.89
Intersection position between first and third aim moment	φ_{ci}	rad	−0.00063
Intersection position between second and third aim moment	φ_{cs}	rad	0.00059

The synthesized cam output parameters are given in Figure 9. The graph of the position output angle ψ calculated using (19) is presented in Figure 9a and pressure angle θ according to (34) is shown in Figure 9b.

(a) (b)
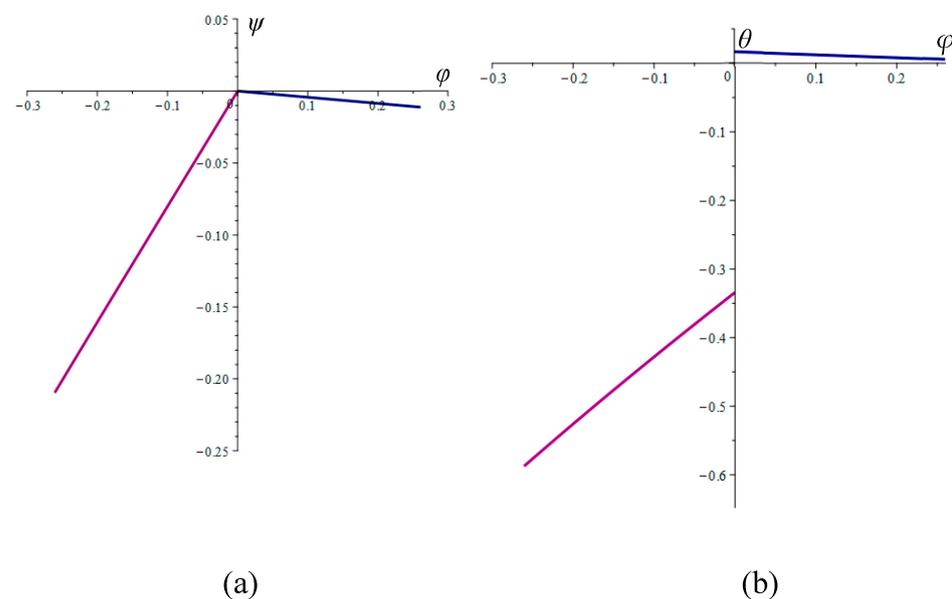
Figure 9. The output parameters of the involute cam: (**a**) The position output angle ψ [rad]; (**b**) The pressure angle θ [rad].

In Figure 10, the graphs of the obtained recuperative moment M_r compared to the reference recuperative moment M_r^* are shown. Small variations in the extreme values and slopes of the two moments are observed, but they do not have a significant impact. The actual function that generates the cam can be considered a satisfactory engineering solution for the intended drive.
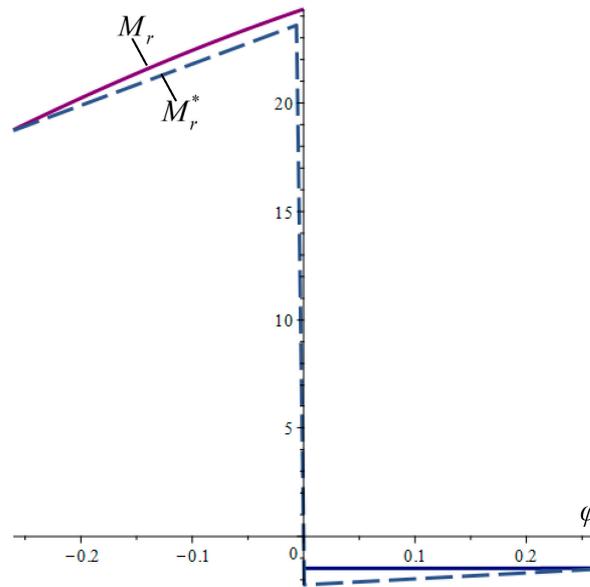
Figure 10. The graph of the synthesized recuperative moment M_r compared to the reference recuperative moment M_r^*.

The synthesis conditions are fully met by the obtained results. The stiffness k_r of the newly obtained recuperative spring is 9947.7 N/m which is compared with the design in Figure 10 and the results obtained in [32] show about 250 times reduction. This means that in the newly synthesized mechanism, the reactions among mechanism parts will have relatively small magnitudes.

6. Choice of the SMA Wire Parameters

In order to enhance the reliability of the pump, a strain of 2.5% was selected for the SMA wires, followed by determining their appropriate length:

$$l_{SMAI} = l_{SMAS} = \frac{r_M \sin \varphi_0}{0.025} \tag{37}$$

where l_{SMAI} l_{SMAS} is the length of the discharge and suction SMA wires, $r_M = OM$. The above formula is valid if distance OF is chosen to be equal to r_M.

The diameter of the SMA wires depends on the maximal absolute values of the total moments M_{T1m} and M_{T2m} obtained in Figure 3b,c.

$$d_{SMAI} \geq \sqrt{\frac{4M_{T1M}}{\pi r_M [\sigma]}} \quad d_{SMAS} \geq \sqrt{\frac{4M_{T2M}}{\pi r_M [\sigma]}} \tag{38}$$

where d_{SMAI} and d_{SMAS} are the diameters of the SMA discharge and suction wires, respectively, and $[\sigma]$ is a permissible normal stress of SMA.

The thermal time constant τ_T [37,38] is determined by the equation

$$\tau_T = \frac{\rho_s V_s c_p}{A_s h_c} \tag{39}$$

where ρ_s is the density of the SMA wire, V_s is the volume of the SMA wire, c_p is the specific heat of the SMA wire, h_c is the heat transfer coefficient for convection between air and the NiTi SMA wire, and A_s is the surface area of the wire. To decrease the convection heat transfer, instead of one wire n branches of wires of smaller diameter d_b with the same pulling force are used, or $d_b = \frac{1}{\sqrt{n}} d_{SMA}$ where d_{SMA} is the diameter of any nonbranched or one-branch SMA wire.

Taking into account that $V_s = \frac{\pi d_{SMA}^2 l_{SMA}}{4}$ and $A_s \approx \pi d_{SMA} l_{SMA}$, the thermal time constant is transformed in

$$\tau_T \approx \frac{\rho_s d_b c_p}{\sqrt{n} h_c} \tag{40}$$

The piston's speed is influenced by the number of branches of the applied SMA wires, as shown in this result. The thermal time constant does not depend on the length l_{SMA} of the SMA wire but is proportional to its diameter and inversely proportional to the square root of the number of branches.

7. Conclusions

In this research, a novel design of a bistable piston pump is proposed, incorporating SMA wire, a two-section involute cam, and a recuperating spring. Through a comprehensive analysis and type, force, and geometry synthesis, this study significantly contributes to the understanding and development of the bistable piston pump driven by SMA and an energy-recuperating spring.

The recuperating mechanism is implemented by employing a two-section involute cam that features a cusp point to determine the unstable position of the pump. Throughout each suction or discharge period, an SMA wire serves as the initial driving force, causing the rotation of the cam as it passes through the cusp point. Subsequently, the recuperating spring takes charge of the drive and completes the remaining stroke.

This study uncovers the fundamental kinematic and force relationships of a cam mechanism employing a two-section involute profile. The development of the two-section involute cam synthesis entails determining the dimensions and profile of the cam, as well as deriving the relationship between the output angle of the oscillating cam follower and the force pressure angle. The numerical investigations demonstrate that a cam composed of two involute profiles can produce a moment based on a prescribed reference discontinuous function, with extrema of opposing signs. The synthesis of a bistable mechanism with a two-section involute cam results in a spring stiffness reduction of 250 times compared to a similar mechanism proposed in reference [32].

By considering the number of branches in the SMA wires, a relationship for the thermal time constant is derived. It has been established that the thermal time constant remains independent of the wire's length while exhibiting a direct proportionality to its diameter and an inverse proportionality to the square root of the number of branches. This relationship provides an opportunity to control the dynamic response of the structure by adjusting the parameters of the SMA wires.

The findings of this research can be applied to assess the potential for enhancing the performance of the pump. They hold promise for enhancing the overall performance and efficiency of pump mechanisms in a wide range of applications, particularly those that necessitate precise control and energy-saving capabilities. The synthesis method presented in this study has extensive applications as it enables the combination of actuation through a two-section involute cam with various other types of actuation, including solenoids, magnetostrictive, hydraulic and pneumatic actuation, piezoelectric, capacitive, thermoelectric, etc.

In our forthcoming research, we will employ the proposed synthesis method to construct a physical prototype of the studied pump, incorporating a two-section involute cam. Following that, we will conduct comprehensive experimental studies, including efficiency testing.

Author Contributions: Conceptualization, M.K., T.T., G.T., R.M., and K.K.; validation, T.T. and M.K.; formal analysis, M.K., T.T., G.T., R.M., and K.K.; investigation, M.K., T.T., G.T., R.M., and K.K.; resources, T.T. and M.K.; writing—original draft preparation, M.K., T.T., G.T., R.M., and K.K.; writing—review and editing, M.K., T.T., and R.M. All authors have read and agreed to the published version of the manuscript.

Institutional Review Board Statement: Not applicable.

Data Availability Statement: Not applicable.

Conflicts of Interest: The authors declare no conflict of interest.

References

1. Leo, D.J. *Engineering Analysis of Smart Material Systems*; John Wiley & Sons, Inc.: Hoboken, NJ, USA, 2007.
2. Trehern, W.; Ortiz-Ayala, R.; Atli, K.C.; Arroyave, R.; Karaman, I. Data-driven shape memory alloy discovery using Artificial Intelligence Materials Selection (AIMS) framework. *Acta Mater.* **2022**, *228*, 117751. [CrossRef]
3. Zhang, J.; Ke, X.; Gou, G.; Seidel, J.; Xiang, B.; Yu, P.; Liang, W.I.; Minor, A.M.; Chu, Y.H.; Van Tendeloo, G.; et al. A nanoscale shape memory oxide. *Nat. Commun.* **2013**, *4*, 2768. [CrossRef] [PubMed]
4. Lee, S.; Cheng, C.; Guo, H.; Hippalgaonkar, K.; Wang, K.; Suh, J.; Liu, K.; Wu, J. Axially Engineered Metal–Insulator Phase Transition by Graded Doping VO2 Nanowires. *J. Am. Chem. Soc.* **2013**, *135*, 4850–4855. [CrossRef] [PubMed]
5. Liu, Y.; Humbeeck, J.; Stalmans, R.; Delaey, L. Some aspects of the properties of NiTi shape memory alloy. *J. Alloys Compd.* **1997**, *247*, 115–121. [CrossRef]
6. Naresh, C.; Bose, P.S.C.; Rao, C.S.P. Shape memory alloys: A state of art review. *IOP Conf. Ser. Mater. Sci. Eng.* **2016**, *149*, 012054. [CrossRef]
7. Otsuka, K.; Wayman, C.M. *Shape Memory Materials*; Cambridge University Press: Cambridge, UK, 1998.
8. Duerig, T.W.; Melton, K.N.; Stockel, D.; Wayman, C.M. *Engineering Aspects of Shape Memory Alloys*; Butterworth-Heinemann: Oxford, UK, 1990; p. 499.
9. Kahn, H.; Huff, M.A.; Heuer, A.H. The TiNi shape-memory alloy and its applications for MEMS. *J. Micromech. Microeng.* **1998**, *8*, 213. [CrossRef]
10. Bellouard, Y. Shape memory alloys for microsystems: A review from a material research perspective. *Mater. Sci. Eng. A* **2008**, *481*, 582–589. [CrossRef]
11. Fu, Y.; Luo, J.; Ong, S.; Zhang, S.; Flewitt, A.; Milne, W. A shape memory microcage of TiNi/DLC films for biological applications. *J. Micromech. Microeng.* **2008**, *18*, 035026. [CrossRef]
12. Liang, C.; Rogers, C.A. Design of Shape Memory Alloy Actuators. *J. Mech. Des.* **1992**, *114*, 223–230. [CrossRef]
13. Mohammad, H. *Elahinia, Shape Memory Alloy Actuators: Design, Fabrication, and Experimental Evaluation*; John Wiley & Sons: Hoboken, NJ, USA, 2016; pp. 85–124.
14. Majima, S.; Kodama, K.; Hasegawa, T. Modeling of shape memory alloy actuator and tracking control system with the model. *IEEE Trans. Control. Syst. Technol.* **2001**, *9*, 54–59. [CrossRef]
15. Soother, D.K.; Daudpoto, J.; Chowdhry, B.S. Challenges for practical applications of shape memory alloy actuators. *Mater. Res. Express* **2020**, *7*, 073001.
16. Mitrev, R.; Todorov, T.; Fursov, A.; Ganev, B. Theoretical and experimental study of a thermo-mechanical model of a shape memory alloy actuator considering minor hysteresis. *Crystals* **2021**, *11*, 1120. [CrossRef]
17. Concilio, A.; Antonucci, V.; Auricchio, F.; Lecce, L.; Sacco, E. *Shape Memory Alloy Engineering for Aerospace, Structural and Biomedical Applications*; Elsevier: Oxford, UK, 2015.
18. Lagoudas, D. Shape memory Alloys. In *Modeling and Engineering Applications*; Springer: New York, NY, USA, 2008.
19. Abadie, J.; Chaillet, N.; Lexcellent, C.; Bourjault, A. Thermoelectric control of shape memory alloy microactuators: A thermal model. In *Smart Structures and Materials 1999: Mathematics and Control in Smart Structures*; SPIE: Bellingham, WA, USA, 1999. [CrossRef]
20. Le, H.M.; Do, T.N.; Phee, S.J. A survey on actuators-driven surgical robots. *Sens. Actuators A Phys.* **2016**, *247*, 323–354. [CrossRef]
21. Zhu, J.; Liang, N.G.; Huang, W.M.; Liew, K.M. Energy conversion in shape memory alloy heat engine part II: Simulation. *J. Intell. Mater. Syst. Struct.* **2001**, *12*, 133–140. [CrossRef]
22. Dana, A.; Vollach, S.; Shilo, D. Use the Force: Review of High-Rate Actuation of Shape Memory Alloys. *Actuators* **2021**, *10*, 140. [CrossRef]
23. Chi, Y.; Li, Y.; Zhao, Y.; Hong, Y.; Tang, Y.; Yin, J. Bistable and Multistable Actuators for Soft Robots: Structures, Materials, and Functionalities. *Adv. Mater.* **2022**, *34*, 2110384. [CrossRef]
24. Opdahl, P.G.; Jensen, B.D.; Howell, L.L. An Investigation into Compliant Bistable Mechanisms. In Proceedings of the ASME 1998 Design Engineering Technical Conferences. Volume 1B: 25th Biennial Mechanisms Conference, Atlanta, GA, USA, 13–16 September 1998; V01BT01A046. ASME: New York, NY, USA, 1998. [CrossRef]
25. Cao, Y.; Derakhshani, M.; Fang, Y.; Huang, G.; Cao, C. Bistable Structures for Advanced Functional Systems. *Adv. Funct. Mater.* **2021**, *31*, 2106231. [CrossRef]
26. Zhao, J.; Yang, Y.; Wang, H.; Jia, J. A Novel Magnetic Actuated Bistable Acceleration Switch with Low Contact Resistance. *IEEE Sensors J.* **2010**, *10*, 869–876. [CrossRef]

27. Jia, Y. Review of nonlinear vibration energy harvesting: Duffing, bistability, parametric, stochastic and others. *J. Intell. Mater. Syst. Struct.* **2020**, *31*, 921–944. [CrossRef]

28. Rossiter, J.; Stoimenov, B.; Mukai, T. A Bistable Artificial Muscle Actuator. In Proceedings of the 17th IEEE International Symposium on Micro-Nanomechatronics and Human Science, Nagoya, Japan, 6–8 November 2006; pp. 35–40.

29. Scholtes, D.; Seelecke, S.; Rizzello, G.; Motzki, P. Design of a Compliant Industrial Gripper Driven by a Bistable Shape Memory Alloy Actuator. *Am. Soc. Mech. Eng.* **2020**, *84027*, V001T04A001.

30. Kostov, M.S.; Todorov, T.S.; Milkov, M.J.; Penev, I.R. Bistable Valve Actuator. UK Patent Application GB 2558616; No: 1700422.7, 18 July 2018. pending.

31. Todorov, T.; Mitrev, R.; Penev, I. Force Analysis and Kinematic Optimization of a Fluid Valve Driven by Shape Memory Alloys. *Rep. Mech. Eng.* **2020**, *1*, 61–76. Available online: https://www.rme-journal.org/index.php/asd/article/view/8/7 (accessed on 16 July 2023).

32. Kostov, M.; Todorov, T.; Mitrev, R.; Kamberov, K.; Nikolov, R. A Study of a Bistable Reciprocating Piston Pump Driven by Shape Memory Alloys and Recuperative Springs. *Actuators* **2023**, *12*, 90. [CrossRef]

33. Kostov, M.S.; Todorov, T.S. A Bistable Compressor Driven with Shape Memory Alloys for Refrigerator. UK Patent Application GB2207547.7, 2022. pending.

34. Hartenberg, R.S.; Denavit, J. *Kinematic Synthesis of Linkages*; McGraw-Hill, Inc.: New York, NY, USA, 1964; pp. 132–138.

35. Shaw, F.W. Equations for the Design of Involute Cams. *Prod. Eng.* **1933**, *4*, 131.

36. Rothbart, H.A. *Cam Design Handbook*; McGraw-Hill: New York, NY, USA, 2004.

37. Mitrev, R.; Atamas, E.; Goncharov, O.; Todorov, T.S.; Yatcheva, I.I. Modelling and study of a novel electrothermal oscillator based on shape memory alloys. *IOP Conf. Ser. Mater. Sci. Eng.* **2020**, *878*, 012059. [CrossRef]

38. Mitrev, R.; Todorov, T.; Fursov, A.; Fomichev, V.; Il'in, A. A Case Study of Combined Application of Smart Materials in a Thermal Energy Harvester with Vibrating Action. *J. Appl. Comput. Mech.* **2021**, *7*, 372–381. [CrossRef]